RSC Advances

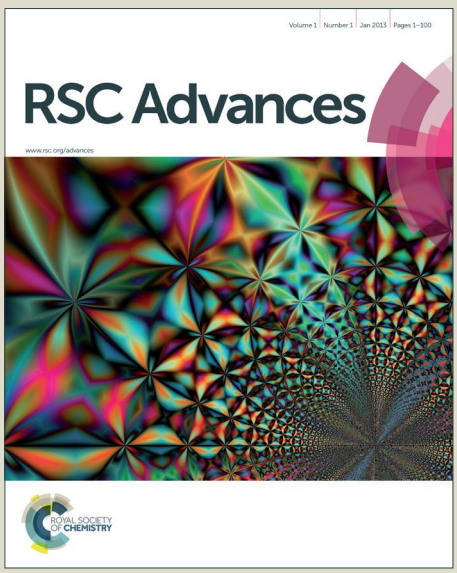

ROYAL SOCIETY OF CHEMISTRY

www.rsc.org/advances

Giant UV-sensitivity in ion beam irradiated nanocrystalline CdS thin films

Pragati Kumar[1]*, Nupur Saxena[1], Sheetal Dewan[1], Fouran Singh[2], and Vinay Gupta[1]

[1]Department of Physics & Astrophysics, University of Delhi, Delhi, India-110 007, India

[2]Inter University Accelerator Centre, Aruna Asaf Ali Marg, New Delhi, 110 067, India

[*]*E*-mail: *pkumar.phy@gmail.com*

*Pragati Kumar, (Corresponding Author)
Department of Physics & Astrophysics,
University of Delhi-110007, India
Phone No.: +91 9555356441,
Fax No.: +91 11-27667036
E-mail: pkumar.phy@gmail.com

Nupur Saxena,
Department of Physics & Astrophysics,
University of Delhi-110007, India

Sheetal Dewan
Department of Physics & Astrophysics
University of Delhi, Delhi-110 007, India,

Fouran Singh,
Inter University Accelerator Center,
Aruna Asaf Ali Marg,
P.O. Box 10502, New Delhi-110067, India

Vinay Gupta
Department of Physics & Astrophysics
University of Delhi, Delhi-110 007, India,

Abstract

A highly sensitive UV-detector is devised for the first time from ion beam irradiated nanocrystalline CdS (nc-CdS) thin films. The UV-sensors are fabricated using pulsed laser deposited nc-CdS thin film on Si wafer and subsequent irradiation treatment. The swift heavy ion irradiation (SHII) of nc-CdS thin films is carried out using 70 MeV $^{58}Ni^{6+}$ ions. The sensors used in present study are easy to fabricate and require inexpensive materials, they feature characteristics similar to those of UV sensors designed with complex structures and expensive procedures. Current-voltage (*I-V*) measurements reveal enrichment in carrier concentration and improvement in conductivity under the exposure of SHI. The giant conductivity may be attributed to the enhancement in sulfur vacancies as consequence of SHII. The senor exhibits improvement in responsivity, photosensitivity, and efficiency as a function of ion fluence and attain maximum values as ~ 53 W/A, 576.4 % and 15.6×10^3 % respectively for the film irradiated at fluence 1×10^{13} ion/cm^2. The response time of the sensor reduces with increase in ion fluence and becomes minimum (rise time 165 ms and fall time 65 ms at 3V) for the same sensor. The possible mechanism involved for SHII induced moderation in conductivity and consequently photosensitivity is explained on the basis of variation in defect densities.

Key Words: Nanocrystalline CdS thin films, pulsed laser deposition, ion beam irradiation, defect density, UV-sensor.

▪ INTRODUCTION

Over the past two decades, one, two and three or zero dimensional semiconductor nanostructures (SNs) are serving as model materials to understand basic physical phenomena at nano-dimensions and for fabrication of nanoscale devices including solar cells, nanolaser, light emitting diodes (LEDs), and photodetectors with improved performance and operating

conditions.[1] SNs are believed to be excellent building blocks for the next generation of highly sensitive and selective sensors because of their high surface-to-volume ratio and multifunctionality.[2] Immense efforts have been made for the advancement of photosensors owing to the diverse applications of photodetectors as binary switches in imaging techniques, light-wave communications, as well as in future memory storage and optoelectronic circuits in which the operation is based on the measurement of their optoelectronic response to incident radiation.[3] Particularly, detection of ultra-violet (UV) radiation out of electromagnetic spectrum concerns superfluous attention because of its primary obligation in many commercial, military and scientific areas such as ozone layer monitoring, flame detection, missile warning systems, medicine, astronomy, and UV based skin therapies etc.[4] Out of all three categorized UV (UV-A, B and C) spectra, overexposure of UV-A radiations is the most hazardous to living beings. Furthermore, the exposure of UV radiations leads to erythema, premature aging and skin pigmentation.[5] Still, microelectronic industries require use of UV-A (λ=400-320 nm) radiations for patterning. Therefore, UV radiation detection is one of the prime necessities of current scenario which demands development of efficient, stable and fast speed ultraviolet (UV) photodetectors.

To date, number of SNs has been used in UV-detectors and the mechanism involved in photodetection has also been uncovered to some extent.[3-17] Cadmium sulfide (CdS) with its direct bandgap (for bulk CdS ~2.42 eV) is one of the most studied metal chalcogenide semiconductor because of its relatively low work function, large refractive index, outstanding emission in visible range and excellent thermal and chemical stability. The excellent electronic and optical properties of CdS have been exploited for the development of solar cells,[18] LEDs,[19] photodetectors,[8, 9] waveguide,[20] electrochemiluminescence sensor,[21] bio-imaging,[22] and lasers.[23]

Diverse approaches have been applied to improve the photoconductivity and thereby UV-sensitivity of SNs including composition and band gap engineering,[1, 6] formation of alloy layers,[9, 10] field effect transistor,[1, 6, 11] impurity incorporation,[24] peizo-phototronic,[25] formation of heterostructure,[25, 26] formation of schottky contact[12] etc. However, there has been negligible concern on influence of post deposition treatments viz. annealing and swift heavy ion irradiation (SHII) on the modification of photosensing materials and devices. Recently, Shaikh et al.[27] studied the current voltage (*I-V*) characteristics of 250 ºC annealed CdS–Bi_2S_3 bi-layer thin film and film irradiated by 120 MeV Au^{9+} ions at a particular fluence 5×10^{12} ions/cm^2 under white light illumination. They have obtained 28% photosensitivity for the irradiated film. Though, a systematic study of SHII with varying fluence to induce material modifications for photodetection is rarely performed. Here, it is noticeable that the scope of ion beam induced multifunctionality has been extended for diverse applications including gas sensing,[28] photodiode,[29] thermoelectricity[30] along with material engineering and characterization in recent years. The underlying consequences of SHII such as defect engineering,[31, 32] nanostructure formation,[33] crystal lattice engineering,[34, 35] high pressure phase generation[36] etc. are responsible for these advancements. "SHII leads to many fold advantages over conventional thermal annealing/Laser annealing/rapid thermal annealing as; (1) the particle size can be increased or reduced i.e. controlled depending on the ion beam parameters, (2) one can control the defects (creation/annihilation) in a precise way by selecting ion beam parameters, (3) SHII avoids the possibility of interdiffusion of elements at the material/substrate interface, which usually occurs in the post deposition annealing at elevated temperature, (4) the spatial selectivity (longitudinal as well as lateral) of range of ions in matter i.e. control on depth profiling and distribution."Since SHII can provide a vast range of modifications in the materials, so it is a promising tool to

establish new horizons in designing and fabricating futuristic devices and moderating their performances.

In this article, we have extended the application of SHII to improve the UV sensitivity in nanocrystalline CdS (nc-CdS) thin film sensors in a systematic way for the first time. For this purpose, pulsed laser deposited (PLD) nc-CdS thin films were irradiated with different fluences of 70 MeV Ni ions followed by UV sensing studies at 355 nm laser illumination. Here we have demonstrated that SHII causes increment in carrier concentration, which enhances current and photocurrent with improved photosensitivity. The mechanism involved in carrier concentration enhancement under influence of SHII is discussed considering defect density concentration as an impact of SHII.

▪ EXPERIMENTAL SECTION

Thin films deposition. The detailed procedure for growth of nc-CdS thin films by PLD is described elsewhere.[32] All the samples investigated were synthesized using PLD by guiding a pulsed excimer KrF laser: an ultraviolet source of 248 nm emission onto a target of chemically synthesized CdS quantum dots (QDs).[37] The laser beam of energy 300 mJ/pulse with repetition rate 10 Hz and pulse width of 10 ns was focused onto a rotating target which was kept at a distance of 5.5 cm from n-type single-crystal Si (111) wafer of size 1×1 cm^2 and mounted at an oblique angle of 30° with respect to the incident laser beam. The films were deposited keeping the substrate at 200 ºC inside a stainless steel vacuum chamber keeping the base pressure better than 5×10^{-6} Torr. The thickness of films was ~250 nm.

Swift heavy ion irradiation. To examine the ion beam induced functionality in nc-CdS thin films, irradiation was carried out at different fluences (1×10^{12}-1×10^{14} ions/cm^2) of 70 MeV Ni^{6+} ions using 15 UD Pelletron Accelerator at Inter University Accelerator Centre (IUAC), New Delhi,

India. The SHII was performed inside a chamber with base pressure ~ 2×10^{-6} Torr at room temperature. The ion beam of approx constant current of ~ 1 pnA (particle nano Ampere) was scanned over entire area of film (~ $1\times1cm^2$) with an electromagnetic scanner to ensure the uniform irradiation. The electronic energy loss, nuclear energy loss, and range of the incident 70 MeV Ni ions in CdS were simulated using electronic stopping, nuclear stopping and range of ions in matter (SRIM),[38] and found to be 10.58 keV/nm, 0.031 keV/nm and 10.94 μm, respectively.

Characterizations. The basic characterization (glancing angle x-ray diffraction, micro-Raman, transmission electron microscopy (TEM), UV-visible and photoluminescence (PL) spectroscopy) for structural and optical studies were carried out and are reported elsewhere[32]. In present study Hall measurement is carried out to study the carrier concentration, conductivity, mobility and nature of majority charge carries using ECOPIA-HMS-3000 operating at magnetic field of 0.57 T. To study the surface morphology and grain size atomic force microscopy (AFM) is carried out using Nanoscope IIIa SPM Atomic Force microscope in tapping mode.

UV-sensing measurements. For the UV sensing, metal-semiconductor-metal (M-S-M) structure is employed in symmetric geometry on the pristine and irradiated films using high quality Ag paste. The $I-V$ characteristics of the nc-CdS thin film structures is measured in voltage range -5V to +5V under illumination with UV laser of power 1mW wavelength 355 nm or under dark conditions in ambient air at room temperature using a semiconductor characterization system (Keithley 4200 SCS). The time-dependent photocurrent response under UV laser illumination for the light-on and light-off states is recorded at applied voltages ranging from 1V-5V.

▪ RESULTS AND DISCUSSION

Surface morphology, root mean square (rms) surface and average particle size (APS) of pristine and irradiated films have been investigated by AFM. Figure 1a & b show the two-dimensional micrographs (in 0.5 μm × 0.5 μm scale) of pristine and film irradiated at fluence 1×10^{13} ion/cm^2 respectively. It is evident that the pristine film is comparatively porous with respect to the irradiated one. The irradiated films are uniform, continuous and contain well-distinguished small particles. The corresponding particle size histograms are shown in the insets of each micrograph. The APS and rms roughness of the pristine film is ~ 9.4 nm and ~ 4.9 nm respectively (Figure 1a). It is observed that APS and rms roughness decreases with increase in ion fluence upto 1×10^{13} ion/cm^2 and then increases for highest fluence. The rms roughness values are estimated as ~ 3.2 nm, 2.1 nm, 3.1 nm for the films irradiated at fluence 1×10^{12} ion/cm^2, 1×10^{13} ion/cm^2, and 1×10^{14} ion/cm^2 respectively. UV-Visible absorption spectroscopy is carried out to study the bandgap modification in nc-CdS films as an impact of SHII. Figure1c shows the variation of APS estimated using effective mass approximation employing the bandgaps determined by UV-visible spectroscopy along with the APS estimated by AFM. It is illustrated that the estimated values of APS by the two methods are very close and follow the same trend. The approximately same APS for 1×10^{13} ion/cm^2 irradiated film can be featured in transmission electron micrographs (Figure 1d).

To investigate the variation in electrical transport parameters as an impact of SHII, Hall measurement is carried out. The different parameters obtained from Hall measurement are summarized in Table 1.

It is noticed that the Hall coefficient of all films is negative suggesting that the concentration of electrons is higher than holes i.e. the films are n-type. It is obvious that the electrical resistivity reduces and carrier (electron) concentration increases as a function of irradiation fluence upto

1×10^{13} ion/cm^2 beyond this these two parameters show opposite behavior. The electron concentration for the pristine, 1×10^{12} ion/cm^2, 1×10^{13} ion/cm^2, and 1×10^{14} ion/cm^2 irradiated samples is estimated as 1.18×10^{18}, 1.74×10^{18}, 5.14×10^{18}, and 4.07×10^{18} cm^{-3} respectively. The reduction in electron mobility upon irradiation upto 1×10^{13} ion/cm^2 is due to the rise in defects concentration as consequence of atomic displacement of the Cd or S atoms at substitutional or interstitial sites. Figure 2a, b, & c show the unirradiated film, under the exposure of irradiation and the different possible phenomena during the passage of SHI through the material respectively. The schematic (Figure 2c) shows only some phenomena relevant here out of many other complex phenomena. It can be seen that there is always a prominent chance of creation of vacancy and interstitial by displacement of atom during the passage of SHI through the material. The increase in defect density results in enhancement of inter-collision of charge carriers and thus reduces the mobility of carriers.[39] The schematic of the fabricated sensor is shown in Figure 2d.

I-V characteristics of all samples in dark and under illumination of UV light are shown in Figure 3a-d. It is clear that current rises with increase in ion fluence and becomes maximum at irradiation fluence 1×10^{13} ion/cm^2. The maximum change observed in current for 1×10^{13} ion/cm^2 irradiated sample at 5V is more than an order with respect to the pristine. It is evident that *I-V* characteristics show nearly Schottky behavior. For Schottky diode the total current (I) across metal-semiconductor junction is given as;[40]

$$\ln(I) = \ln(JA) + \ln J_A + V\left(\frac{q}{k_B T} - \frac{1}{E_0}\right) \qquad (1)$$

where J is current density through the barriers, A is contact area associated with barrier, J_A is slowly varying function of applied bias voltage and E_0 is given by

$$E_0 = E_{00}\coth\left(\frac{E_{00}}{k_B T}\right) \qquad (2)$$

where E_{00} is a function of carrier concentration (n) and defined as

$$E_{00} = \frac{hq}{4\pi}\left(\frac{n}{m^*\varepsilon}\right)^{1/2} \quad (3)$$

where m^* is effective mass of electron and ε is dielectric constant. The Schottky behavior of *I-V* characteristics is studied by fitting the experimental data with the above equation and estimated the electron concentration. The electron concentration for the pristine, 1×10^{12} ion/cm^2, 1×10^{13} ion/cm^2, and 1×10^{14} ion/cm^2 irradiated samples is calculated as 1.13×10^{18}, 1.62×10^{18}, 3.73×10^{18}, and 3.11×10^{18} cm^{-3} respectively. It is significant to mention here that electron concentration estimated using above equation is consistent with the values obtained from Hall measurement for pristine and 1×10^{12} ion/cm^2 irradiated samples. Though, there is perceptible divergence in the values of electron concentration for other two samples. It is because of the slight deviation of *I-V* characteristic from Schottky behavior as consequence of increase in electron concentration. The enhancement in electron concentration as a function of ion fluence is ascribed to the rise in sulfur vacancies and thus conductance. Recently we have studied the variation of defect densities as a function of ion fluence and suggested that due to electronic activation as an impact of SHII, Cd and S atoms move from one minimum to the next lower minimum by crossing a potential barrier during recrystallization, leads to enrichment in population density of defects.[32] Since, the displacement of Cd atom to an interstitial position is easier than that of a S atom under high energy electronic bombardment,[41] therefore at lower irradiation fluence (1×10^{12} ion/cm^2) the enhancement in population density of sulfur vacancies (V_s) is relatively very small as compared to that at irradiation fluence 1×10^{13} ion/cm^2, thereby the observed variation in conductance. In contrary, at fluence 1×10^{14} ion/cm^2, it is predicted that the particle size further reduces, causing dissolution of smaller crystals, and growth of larger particles due to Ostwald ripening.[42] The

grain growth results in reduction of surface to volume ratio and hence population density of V_s which ultimately leads to a drop in electron concentration and conductance.

It is obvious from Figure 3a-d that all films show good UV sensitivity under illumination as photocurrent of all samples is higher than their respective dark current. It is manifested that the photocurrent increases by ~ 2.3, 2.9, 6.3, and 4.0 times for pristine, 1×10^{12} ion/cm^2, 1×10^{13} ion/cm^2, and 1×10^{14} ion/cm^2 irradiated samples respectively relative to respective dark current at 5V. The mechanism responsible for enhancement in photocurrent with respect to dark current can be understood as follows. Since there is always a finite content of oxygen present on the surface of each sample due to adsorption of atmospheric oxygen, it leads to charged surface states on CdS by the transfer of conduction electrons to the adsorbed species. The transport of electron generates a compensating space charge layer of ionized donors and a Schottky barrier is created. Under the illumination of UV-light free carriers are created. The free holes so created are engrossed to the surface by the barrier field and these holes are neutralized the negative ions to release the adsorbed gas and the photogenerated electrons are driven into the interior of film by the barrier field enhancing the concentration of electrons in conduction band and lead to boost in conductivity.[43] The entire mechanism of photoconduction can be interpreted as;

$$h\nu \longrightarrow h^+ + e^- \qquad (4)$$

$$h^+ + O_2^-{}_{ads} \longrightarrow O_2 \uparrow \qquad (5)$$

Next, the UV-response characteristics are investigated within the entire range of applied bias voltage (1V-5V). Time dependent UV-sensing at lowest bias voltage 1V is shown for all the prepared sensors in Figure 4a. Repeated cycles for UV ON/OFF mode are displayed in sequential manner. It divulges that the response of different sensors to the incident light is fast and exhibits excellent stability and repeatability. Analytical investigation suggests a rise time (t_r)

of 1100 ms, 600ms, 200 ms & 270 ms and fall time (t_f) of 986 ms, 820 ms, 72 ms & 95 ms for pristine, 1×10^{12} ion/cm^2, 1×10^{13} ion/cm^2, and 1×10^{14} ion/cm^2 irradiated UV-sensors respectively. Though, the minimum response time is achieved at various bias voltages for different sensing devices. However, here in text the response time of different samples only at the lowest bias voltage are mentioned. To calculate the rise and decay time constants; (τ_r) and (τ_d), we tried to fit our experimental data with single exponent of the type;[24] $I = I_0 + Ce^{-t/\tau}$. Fitting reveals that the above equation is unable to proffer good fitting for rising edge, though it offers good fit in trailing edge of experimental data as shown in Figure 4b. Therefore, two exponents of the type; $I = I_0 + C_1e^{-t/\tau_1} + C_2e^{-t/\tau_2}$ with two time constant τ_1 and τ_2 corresponding to shorter and longer time respectively are used to fit the rising edge. Here C_1 and C_2 are scaling constants and τ_1 and τ_2 are related to the charge generation and diffusion of charge carriers respectively. Two time constants for the rising edge can be interpreted considering the porosity of the films, which is well visualized in AFM studies. It can be seen from Figure 1. that the distribution of particles on the surface and rms roughness of pristine film is relatively higher than those of irradiated films indicating relatively larger porosity of pristine film, which results to adsorption of more oxygen on the surface of this film. This enhances the space charge region and built-in-potential near the surface, which blocks the generation of the electron-hole pair and thus higher τ_1 is observed. The less carrier concentration of this film leads to a higher rate of charge diffusion and thus τ_2 is relatively small. We found that the rising edge of experimental data is well described using this equation as shown in Inset Figure 4b. The different parameters estimated from fittings are summarized in Table 2.

In order to evaluate the entire performance of device, crucial parameters such as responsivity (R), external quantum efficiency (η), and sensitivity (S) are further calculated. Mathematically these parameters are defined as;[5]

$$R = \frac{I_p}{P_{in}}, \eta = \frac{hc}{e\lambda} R_\lambda, and\ S = \frac{I_p - I_d}{I_d} \times 100. \quad (6)$$

where I_p is photocurrent, P_{in} incident power, h is Planck's constant, c is velocity of light, e is electronic charge, λ is wavelength of incident light, $R_\lambda = \frac{I_p - I_d}{P_{in}}$ is spectral responsivity, and I_d is dark current. The values of all these parameters are calculated at different bias voltages ranging from 1V to 5V. The variation of responsivity is shown in Figure 5a whereas Inset Figure 5a shows variation in external quantum efficiency as a function of bias voltage. It is evident that both the parameters show nearly linear behavior with bias voltage and attain maximum values at 5V for all sensing devices. The highest achieved values of responsivity and quantum efficiency are ~ 53 A/W and 15.6 × 10^3 % at 5V for 1× 10^{13} ion/cm^2 irradiated sensor. The sensitivity of the UV-sensing device is shown in Figure 5b. It is exemplified that maximum sensitivity of all sensing devices is achieved at diverse biasing voltages. The largest accomplished value of sensitivity is ~ 578.6% for 1× 10^{13} ion/cm^2 irradiated sensor operating at 3V, which is fairly high in context of the existing reports.[27]

The literature on UV-sensors suggests nc-CdS thin films are not much explored as a UV-sensitive material. Though, a variety of ideas have been exploited to improve the performance of UV-sensors, e.g. fabrication using nanowires, nanobelts and nanosheets of CdS and other SNs. To the best of our knowledge the minimum response (rise and fall) time achieved by nc-CdS thin films is few seconds, whereas it is few tens of milliseconds in case of CdS nanobelts. A brief comparison of the various UV-sensing devices is presented in Table 3. A lot of work has been carried out employing ZnO thin films, nanostructures, composites or heterostructure for the

development of UV-sensors. Though, the sensitivity, response time and lower operating voltages have been the leading issues and challenge for the researchers to explore other materials and means to fabricate highly sensitive and faster devices for real time applications. As illustration, Thyagrajan et. al. investigated the artificially introduced defects on graphene surface for the fabrication of gate tunable UV-sensor and achieved the response time in the order of seconds.[11] A wide wavelength photodetector exhibiting fairly sensitive behavior for UV-light is demonstrated by Ali et. al. using indium selenide microwires grown by vapor-solid technique.[13] Shao et. al. fabricated an organic-inorganic hybrid structure to realize UV-sensor with sufficiently reduced response time.[14] A highly selective, visible blind UV-A sensor was devised by Kobayashi et. al. by growing MgCdS/ZnCdS short period superlattice structure using molecular beam epitaxy method.[10] A positive step towards highly responsive and extremely efficient UV-sensor is realized by Zhang et. al. using carbon-fiber/ZnO-CdS double shell microwire with lower applied bias as 2V.[25] In a recent report by Lin et. al., a UV-sensor of exceptional responsivity (~10^5) and detectivity (~10^{16} Jones) at 1 V under the illumination of just 3.5 pW is demonstrated. The sensor can be operated at bias voltage as low as 1mV with remarkable response.[16] Nevertheless, in most of the reports where high sensitivity/efficiency or lower response time/bias voltages are achieved, the device fabrication involves intricate structures that involve tedious steps. Rather, the UV-sensors presented here are in intermediate range as far as the various parameters are concerned alongwith an easy-to-prepare fabrication. The overall performance of present sensing devices is better than most of the reports on nc-CdS thin films,[27, 44] some 1D or 2D CdS nanostructures[2, 12, 15, 17] and even better than recent report on branched CdS/ZnO heterostructures[26] based devices. Conclusively, the sensors proposed here are easy to fabricate and require inexpensive materials, the feature characteristics are similar to those

of UV sensors made with complex and expensive procedures. The present study aims at the exploration of SHII treatment on thin films for enhancing the performance of sensing devices by defect engineering and suggests that ingraining of post deposition treatment (SHII) along with intricate fabrication routes can be applied to further moderate the performance of photosensing devices. Further experiments with different ion beam parameters may lead to astonishing improvement in UV-sensing device scenario.

CONCLUSION:

In summary here we demonstrated the application of SHII to improve the overall performance of CdS thin film based UV-sensors. SHII is a versatile tool to enlarge the population density of defects (V_s) and thereby the carrier concentration which results increment in conductivity of device. The maximum upgrading in conductivity is around two times with maximum 63 times increment in photocurrent at only 1V for 1×10^{13} ion/cm^2 irradiated film with respect to the unirradiated film. In present study we illustrate that the responsivity, quantum efficiency and sensitivity of sensing device are improved by 55 times, 3 times and 80 times at 1V for 1×10^{13} ion/cm^2 irradiated film than that for unirradiated one. It is observed that the response time of sensing device reduces from thousands of millisecond to tens of millisecond by the impact of SHII. Present study opens new doors for the researchers to improve the intact action of sensing devices.

ACKNOWLEDGMENT

The authors (PK: F.4-2/2006(BSR)/PH/13-14/0055 & NS: F.13-905/2013(BSR)) are thankful to University Grant Commission (UGC), India for providing Dr. D. S. Kothari post doctoral fellowship. Dr. Ramesh Chandra, Institute Instrumentation Center, Indian Institute Technology (IIT), Roorkee, India is gratefully acknowledged for providing thin film deposition facility. The

team work done by the pelletron group, IUAC, New Delhi, India during irradiation experiment are highly appreciable.

REFERENCES:

1. L. Li, H. Lu, Z. Yang, L. Tong, Y. Bando, and D. Golberg, *Adv. Mater.,* 2013, 25, 1109.
2. J. S. Jie, W. J. Zhang, Y. Jiang, X. M. Meng, Y. Q. Li, and S. T. Lee, *Nano Lett.,* 2006, 6, 1887.
3. H. Wang, A. Pyatenko, N. Koshizaki, H. Moehwald, and D. Shchukin, *ACS Appl. Mater. Interfaces* 2014, 6, 2241.
4. Z. Q. Xu, H. Deng, J. Xie, Y. Li, and X. T. Zu, *Appl. Surf. Sci.,* 2006, 253, 476.
5. E. Monroy, F. Omn`es, and F. Calle, *Semicond. Sci. Technol.,* 2003, 18, R33.
6. T. Xie, G. Liu, B. Wen, J. Y. Ha, N. V. Nguyen, A. Motayed, and R. Debnath, *ACS Appl. Mater. Interfaces,* 2015, 7, 9660.
7. B. D. Boruah, A. Mukherjee, S. Sridhar, and A. Misra, *ACS Appl. Mater. Interfaces,* 2015, 7, 10606.
8. K. Deng, and L. Li, *Adv. Mater.,* 2014, 26, 2619.
9. M. Enami, K. Tsutsumi, F. Hirose, S. Katsuta, and M. Kobayashin, *Jpn. J. Appl. Phys.,* 2003, 42, L 1047.
10. M. Kobayashi, J. Ueno, M. Enami, S. Katsuta, A. Ichiba, K. Ogura, K. Onomitsu, and Y. Horikoshi, *Journal of Crystal Growth,* 2005*,* 278, 273.
11. K. Thiyagarajan, B. Saravanakumar, and S. J. Kim, *ACS Appl. Mater. Interface,* 2015, 7, 2171.

12. T. Y. Wei, C. T. Huang, B. J. Hansen, Y. F. Lin, L. J. Chen, S. Y. Lu, and Z. L. Wang, *Appl. Phys. Lett.,* 2010, 96, 013508.
13. Z. Ali, M. Mirza, C. Cao, F. K. Butt, M. Tanveer, M. Tahir, I. Aslam, F. Idrees, and M. Safdar, *ACS Appl. Mater. Interface,* 2014, 6, 9550.
14. D. Shao, M. Yu, H. Sun, G. Xin, J. Lian, and S. Sawyer, *ACS Appl. Mater. Interface,* 2014, 6, 14690.
15. M. A. Mahdi, J. J. Hassan, S. S. Ng, Z. Hassan, and N. M. Ahmed, *Physica E* 2012, 44, 1716.
16. K. T. Lin, H. L. Chen, Y. S. Lai, Y. L. Liu, Y. C. Tseng, and C. H. Lin, *ACS Appl. Mater. Interface,* 2014, 6, 19866.
17. T. Gao, Q. H. Li, and T. H. Wang, *Appl. Phys. Lett.,* 2005, 86, 173105.
18. T. K. Todorov, O. Gunawan, T. Gokmen, and D. B. Mitzi, *Prog. Photovolt: Res. Appl.,* 2013, 21, 82.
19. Z. Yang, J. Xu, P. Wang, X. Zhuang, A. Pan, and L. Tong, *Nano Lett.,* 2011, 11, 5085.
20. J. Xu, X. Zhuang, P. Guo, Q. Zhang, W. Huang, Q. Wan, W. Hu, X. Wang, X. Zhu, C. Fan, Z. Yang, L. Tong, X. Duan, and A. Pan, *Nano Lett.,* 2012, 12, 5003.
21. F. Sun, F. Chen, W. Fei, L. Sun, and Y. Wu, *Sensors and Actuators B,* 2012, 166–167, 702.
22. P. Kumar, D. Kukkar, A. Deep, S. C. Sharma, and L. M. Bharadwaj, *Adv. Mat. Lett.,* 2012, 3, 471.
23. J. Lu, X. Lim, M. Zheng, S. G. Mhaisalkar, and C. H. Sow, *ACS Nano,* 2012, 6, 8298.

24. D. Joung, M. Arif, S. Biswas, S. Kar, S. Santra, and S. I. Khondaker, *Nanotechnology,* 2009, 20, 445204.

25. F. Zhang, S. Niu, W. Guo, G. Zhu, Y. Liu, X. Zhang, and Z. L. Wang, *ACS Nano,* 2013, 7, 4537.

26. C. Zhang, W. Tian, Z. Xu, X. Wang, J. Liu, S. L. Li, D. M. Tang, D. Liu, M. Liao, Y. Bando, and D. Golberg, *Nanoscale,* 2014, 6, 8084.

27. S. U. Shaikh, F. Y. Siddiqui, D. J. Desale, A. V. Ghule, F. Singh, P. K. Kulriya, and R. Sharma, *Rad. Phys. Chem.,* 2015*,* 106, 193.

28. A. A. Sagade, R. Sharma, and I. Sulaniya, *J. Appl. Phys.,* 2009, 105, 043701.

29. J. S. Laird, T. Hirao, S. Onoda, and H. Itoh, *J. Appl. Phys.,* 2005, 98, 013530.

30. S. Gupta, D. C. Agarwal, S. K. Tripathi, S. Neeleshwar, B. K. Panigrahi, A. Jacquot, B. Lenoir, and D. K. Avasthi, *Rad. Phys. and Chem.,* 2013, 86, 6.

31. P. Kumar, N. Saxena, V. Gupta, F. Singh, and A. Agarwal, *J. Appl. Phys.,* 2014, 116, 043517.

32. P. Kumar, N. Saxena, R. Chandra, K. Gao, S. Zhou, A. Agarwal, F. Singh, V. Gupta, and D. Kanjilal, *J. Luminescence,* 2014, 147, 184.

33. N. Saxena, A. Agarwal, D. M. Phase, R. J. Choudhary, and D. Kanjilal, *Physica E,* 2010, 42, 2190.

34. G. Rizza, A. Dunlop, G. Jaskierowicz, and M. Kopcewicz, *Nucl. Instrum. Meth. Phys. Res. B,* 2004, 226, 609.

35. A. Kamarou, W. Wesch, and E. Wendler, *Phys. Rev. B,* 2008, 78, 054111.

36. N. Saxena, P. Kumar, A. Agarwal, and D. Kanjilal, *Phys. Status Solidi A,* 2012, 209, 283.

37. P. Kumar, N. Saxena, F. Singh, and A. Agarwal, *Physica B,* 2012, 407, 3347.

38. See www.srim.org for Stopping and Range of Ions in Matter-2008.

39. P. Veeramani, M. Haris, D. Kanjilal, K. Asokan, and S. M. Babu, *J. Phys. D: Appl. Phys.,* 2006, 39, 2707.

40. F. Singh, B. Chaudhary, V. Kumar, R. G. Singh, S. Kumar, and A. Kapoor, *J. Appl. Phys.,* 2012, 112, 073101.

41. C. Bocchi, and C. Ghezzi, *J. Phys. Chem. Solids,* 1975, 36, 421.

42. P. Kumar, N. Saxena, A. Agarwal, and V. Gupta, *Adv. Mat. Lett.,* 2015, 6, 820.

43. P. Mark, *J. Phys. Chem. Solids,* 1964, 25, 911.

44. U. S. Jadhav, S. S. Kale, and C. D. Lokhande, *Mater. Chem. Phys.,* 2001, 69, 125.

TABLE CAPTIONS:

Table 1: Parameters obtained by Hall measurement.

Table 2: The parameters calculated by fitting of rising and trailing edges by $I = I_0 + C_1 e^{-t/\tau_1} + C_2 e^{-t/\tau_2}$ and $I = I_0 + C e^{-t/\tau}$ equations respectively.

Table 3: Comparison of the photoelectrical parameters of different CdS photosensing structures. Here λ is wavelength of illuminated light, τ_r and τ_f are rise and fall times respectively and η is external quantum efficiency.

FIGURE CAPTIONS:

Figure.1. AFM micrographs in 0.5 μm × 0.5 μm scale of (a) pristine and (b) film irradiated at fluence 1×10^{13} ion/cm^2 (c) average particle size estimated by AFM images and UV-Visible

spectroscopy and (d) TEM image of 1×10^{13} ion/cm^2 irradiated film. (Inset: corresponding particle size distribution histograms).

Figure.2. Schematic of (a) pristine film (b) film under the exposure of SHII (c) various promising phenomena as consequence of passage of SHI through the materials and (d) present UV - Sensor.

Figure.3. Current - Voltage (I-V) characteristic of pristine and irradiated sensing devices in dark (black symbols) and under UV-illumination (red symbols).

Figure.4. (a) Time response of the UV-sensing devices at bias voltage 1V. (b) Trailing edge fit with $I = I_0 + Ce^{-t/\tau}$. Inset rising edge fit with $I = I_0 + C_1e^{-t/\tau_1} + C_2e^{-t/\tau_2}$.

Figure.5. (a) Variation of responsivity as a function of bias voltage (Inset: external quantum efficiency varying with bias voltage) and (b) Photosensitivity of various devices at different bias voltages.

Table 1: Parameters obtained by Hall measurement.

Sample	R_H	μ cm^{2}V^{-1}S^{-1}	σ mho/m	n cm^{-3}
Pristine	-5.27	317.1	60.16	1.18×10^{18}
Irradiated at 1×10^{12} ion/cm^2	-3.592	284.1	79.06	1.74×10^{18}
Irradiated at 1×10^{13} ion/cm^2	-1.216	193.4	159.04	5.14×10^{18}
Irradiated at 1×10^{14} ion/cm^2	-1.534	207.7	135.39	4.07×10^{18}

* R_H =Hall coefficient, μ = Mobility, σ = Conductivity, and n= carrier concentration.

Table 2: The parameters calculated by fitting of rising and trailing edges by $I = I_0 + C_1e^{-t/\tau_1} + C_2e^{-t/\tau_2}$ and $I = I_0 + Ce^{-t/\tau}$ equations respectively.

Sample	τ_1 (ms)	τ_2 (s)	τ (ms)
Pristine	117±1	2.25±0.17	748.1±8
Irradiated at 1×10^{12} ion/cm^2	109±1	2.27±0.07	719.9±5
Irradiated at 1×10^{13} ion/cm^2	76±0.5	5.72±0.46	584.7±4
Irradiated at 1×10^{14} ion/cm^2	95±1	4.97±0.53	594.5±6

*τ_1 = rise time constant 1, τ_2= rise time constant 2, and τ = decay time constant.

Table 3: Comparison of the photoelectrical parameters of different CdS photosensing structures.

CdS NSs	Bias Voltage (V)	λ (nm)	τ_r (ms)	τ_f (ms)	Sensitivity /Responsivity	η (%)	Reference
CdS single nanoribbons	1	360	--	--	27%	--	[2]
ZnO Spherical Particles	10	330	--	--	350%	--	[3]
Zn 1−x Mg x O films	1	360	--	--	0.22 A/W	--	[6]
ZnO NWs/ Graphene	8	365	9500	38000	7.3 A/W	2.5×10^{3}	[7]
ZnMgCdS film	10	355	--	--	2 mA/W	--	[9]
MgCdS/ZnCdS superlattices	10	355	--	--	3 mA/W	--	[10]
Defective Graphene FET	V_{bg}-10 V_{ds}-0.01	365	900	1000	18 mA/W	--	[11]
Schottky contact/Ohmic contact CdS Nanowires	-8	365	380 640	380 640	1.8×10^{4} % 1.0×10^{3} %	--	[12]
In_2Se_3 microwire	4	365	110	110	1.0×10^{2} %	--	[13]
Organic Inorganic Hybrid	-10	351	21	23	240A/W	8.5×10^{4}	[14]
CdS nanosheet	1	365	13	15	8.6×10^{2} %	2.9×10^{3}	[15]
nc-CdS film	0.001	365	--	--	74.7 A/W	--	[16]
CdS nanobelts	5	white	1000	3000	--	--	[17]
Carbon-Fiber/ZnO-CdS Double-Shell Microwire	2	372	--	--	1.94×10^{5} A/W	2.87×10^{7}	[25]
Single CdS/ZnO nanobelt Film like configuration	10	405	250 3600	<250 3300	--	--	[26]
CdS–Bi_2S_3 bi-layer films	1	white			43%		[27]
CdS thin films	30	UV	9×10^{5}	9×10^{5}	--	--	[44]
nc-CdS thin film (pristine)	2	355	1012	917	1.59×10^{2}%	5.27×10^{1}	Present Study
nc-CdS thin film (Irr. 1×10^{12} ion/cm^2)	3	355	523	746	1.99×10^{2}%	2.86×10^{2}	Present Study
nc-CdS thin film (Irr. 1×10^{13} ion/cm^2)	3	355	165	65	5.78×10^{2}%	8.44×10^{3}	Present Study
nc-CdS thin film (Irr. 1×10^{14} ion/cm^2)	1	355	270	95	3.24×10^{2}%	7.04×10^{2}	Present Study

* λ = wavelength of illuminated light, τ_r = rise time, τ_f = fall time and η= quantum efficiency.

Graphical Abstract

A highly sensitive UV-detector is devised for the first time from ion beam irradiated nanocrystalline CdS (nc-CdS) thin films. The senor exhibits improvement in responsivity, photosensitivity, and efficiency as a function of ion fluence and attain maximum values as ~ 53 W/A, 576.4 % and 15.6×10^{3} % respectively for the film irradiated at fluence 1×10^{13} ion/cm^{2}. The response time of the sensor reduces with increase in ion fluence and becomes minimum (rise time 165 ms and fall time 65 ms at 3V) for the same sensor.